LAWRENCE
LIVERMORE
NATIONAL
LABORATORY

LLNL-JRNL-648952

The "Churning Mode" of plasma Convection in the Tokamak Divertor Region

D. D. Ryutov, R. H. Cohen, W. A. Farmer, T. D. Rognlien, M. V. Umansky

January 29, 2014

Physica Scripta

Disclaimer

LLNL-JRNL-648952

The "Churning Mode" of plasma convection in the tokamak divertor region

D.D. Ryutov, R.H. Cohen, W.A. Farmer[1], T.D. Rognlien, M.V. Umansky

Lawrence Livermore National Laboratory, Livermore, CA 94551, USA

Abstract

The churning mode can arise in a toroidally-symmetric plasma where it causes convection in the vicinity of the poloidal field null [D.D. Ryutov, R.H. Cohen, T.D. Rognlien, M.V. Umansky, "Favorable effects of turbulent plasma mixing on the performance of innovative tokamak divertors," BAPS **58**, #16, p. 394.]. The mode is driven by the toroidal curvature coupled with a pressure gradient. The toroidal equilibrium conditions cannot be easily satisfied in the virtual absence of the poloidal field (PF) – whence the onset of this mode, which "churns" the plasma around the poloidal field null without perturbing the strong toroidal field. We find the conditions under which this mode can be excited in magnetic configurations with first-, second-, and third-order PF nulls (i.e., in the geometry of standard, snowflake and cloverleaf divertors). The size of the affected zone in second- and third-order-null divertors is much larger than in a standard divertor. The proposed phenomenological theory allows one to evaluate observable characteristics of the mode, in particular the frequency and amplitude of the poloidal field perturbations. The mode spreads the tokamak heat exhaust between multiple divertor legs and may lead to a broadening of the plasma width in each leg. The mode causes much more intense convection in the poloidal plane than the classical plasma drifts.

Keywords: tokamak, divertor, convection, turbulence

---

[1] Also at University of California Los Angeles, Los Angeles, California 90095, USA

1. Introduction

An area of a weak poloidal magnetic field near the null-point of a tokamak divertor possesses interesting equilibrium and stability properties that may significantly affect the divertor performance. It is well known that in the absence of a poloidal field, equilibria in axisymmetric toroidal fields are possible only for trivial pressure distributions, where the pressure is constant on surfaces of nested cylinders with an axis coinciding with the geometrical axis of a tokamak (e.g., [1]). However, such equilibria are incompatible with the pressure distributions in the divertor area, where the pressure varies roughly in the direction parallel to the geometrical axis, from the higher pressure in the plasma confinement zone to the lower pressure towards the divertor targets (Fig. 1).

It was conjectured in Refs. 2-4 that the loss of plasma equilibrium near the poloidal field null may lead to the onset of plasma convection that spreads the heat flux over the whole zone of a weak poloidal field; the plasma then enters a stronger poloidal field in the divertor legs and flows to the divertor targets. A strong plasma convection near the null means that, in the case of divertors with 4 or 6 divertor legs, like the snowflake and cloverleaf, respectively, the plasma fills all of them, leading to increase of a number of strike points from 2 to 4 or 6. In addition, broadening of the plasma distribution in each of the legs may occur.

A mode that we consider here is a large-scale mode of sheared poloidal rotation around the null that brings the hotter plasma adjacent to the confinement zone in the downward direction, thereby allowing for the plasma to flow into additional divertor legs (Fig. 1). The free energy for this convection mode comes from the vertical pressure gradient that is sustained by the heating of the plasma in the upper confinement zone and its cooling

(by the heat flow to the divertor targets) from the bottom. This mode is toroidally-symmetric and does not perturb the toroidal magnetic field, similar to what was assumed in Refs. 5 and 6. It causes poloidal rotation of the whole toroidal flux tube around the null point where the poloidal field is weak. We call this (nonlinear) convective motion the "churning mode."

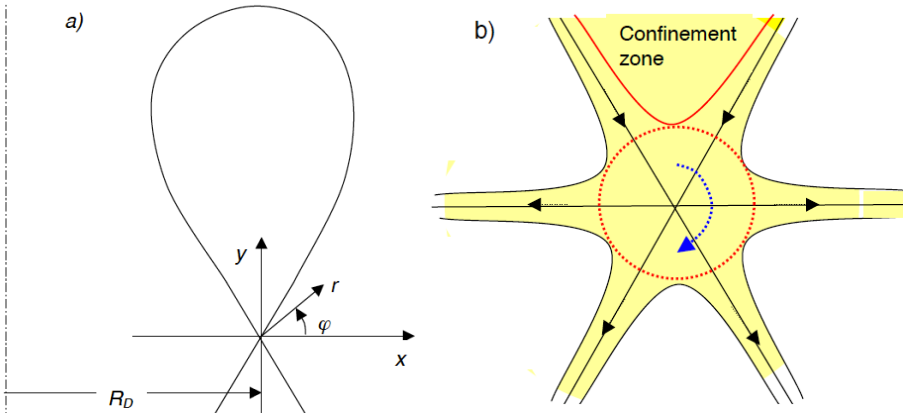

Fig. 1 The geometry of the system for the case of a snowflake divertor: a) the overall configuration; b) The structure of the weak poloidal field zone near the null; dashed red circle encloses the convection zone with blue dashed arrow indicating the initial direction of rotation; solid red line inside the confinement zone shows the area inside the separatrix affected by convection; in the equatorial plane this layer becomes quite narrow, see discussion around Eq. (29).

In this note we add a quantitative element to a heuristic assessment of the convection problem presented in Refs. 3-5. A discussion outlined below is still partially heuristic, not providing a full self-consistent picture of the plasma convection, but several significant elements of the problem are analyzed quantitatively, allowing one to make more reliable predictions regarding the onset and intensity of the churning mode convection.

Note that enhanced plasma transport near the PF null can also appear as a result of instabilities of the plasma equilibrium in the cases where such an equilibrium exists. This

side of the problem was briefly discussed in Ref. [5]. A detailed analysis of the flute-like mode (that does not perturb the toroidal field but does perturb the poloidal field) was presented in Ref. [6]. A small-scale ballooning mode may exist on the field lines that make many toroidal revolutions before leaving the weak poloidal field zone [7]. Refs. 6, 7 contain estimates of the critical beta leading to the excitation of these modes.

The plasma poloidal convection near the null can also be driven by an equilibrium electric field normal to poloidal flux surfaces. This mechanism has been analyzed in Ref. 8 for a standard divertor and in Ref. 9 for the snowflake divertor.

The "activation" of additional divertor legs has been observed experimentally in all three tokamaks (TCV, NSTX and DIII-D) where a snowflake divertor configuration has been studied [10-14] The effect was strongest during the ELM events [10-14]. Numerical simulations of the plasma transport of the snowflake divertor using the EMC3 code [15] indicate that, in order to reach at least qualitative agreement with experimental results of the TCV facility, one needs to increase the transport near the null by orders of magnitude compared to the "normal" transport typically assumed in scrape-off layer (SOL) simulations (a sizable fraction of Bohm transport). These facts serve as strong motivation for looking for new transport mechanisms near the poloidal field null.

In numerical estimates throughout the paper we will use a set of parameters for some generic mid-size tokamak (Table 1). The zone near the poloidal field null is not very amenable to direct measurements, and it is probably premature to make direct application of our results to specific devices. Still, our estimates for a generic case may help to guide a discussion of specific experiments.

Table 1. Parameters of a generic mid-size tokamak used in the numerical estimates

Parameter	Major radius	Minor radius	Toroidal field	Midplane poloidal field (PF)	Plasma dens.in conv. zone	Plasma temp.in conv. zone
Notation	R, cm	a, cm	B_T, T	B_{pm}, T	n, cm^{-3}	T, eV
Value	150	60	2	0.25	10^{13}	50

The further presentation is organized as follows. In Sec. 2 we introduce notation and present expressions for the poloidal magnetic field for the three configurations (standard, snowflake and cloverleaf). In Sec. 3 we describe the general structure of the churning mode. In Sec. 4 we evaluate the thermal energy release by a plasma poloidal rotation around the poloidal field null-point. The condition that a strong toroidal field is not perturbed makes the energy release proportional to the toroidal curvature. In Sec. 5 we evaluate the perturbation of the poloidal field magnetic energy assuming infinite plasma electrical conductivity (a condition that typically reflects the real situation quite well). In Sec. 6, we compare the two energies and, based on that, evaluate the size of the convection zone for various magnetic configurations. Section 7 contains evaluation of the dynamic characteristics of the mode, in particular, its turn-over time. Finally, Sec. 8 contains a summary and outlook.

2. The magnetic geometry

The magnetic field structure for a snowflake divertor is illustrated in Fig. 1a. The geometric axis is the dash-dotted line to the left; the major radius corresponding to the null point is R_D. We use Cartesian coordinates (x,y) in the poloidal plane, with the axis x collinear to the major radius. Alternatively, a polar system (r,φ) is used with the angle φ

measured counter-clockwise from the x axis. We consider the vicinity of the null point, therefore assuming $r<<R_D$. An expanded view of the zone near the null is shown in Fig. 1b, where not only the anticipated convection zone is shown, but also a SOL and four outgoing divertor legs. On average, there is certainly a plasma pressure gradient in this area, with a higher pressure above the null and lower pressure below the null. The magnitude of this gradient defines the size of the zone where the churning mode can be active. In the absence of such a gradient, the drive for the churning mode would not be present

Although in Fig. 1a we have shown field lines of the poloidal magnetic field in the whole domain, including the immediate vicinity of the null, the poloidal field throughout this region is weak. We shall find the size of the zone where the field is so weak that the plasma equilibrium loses any semblance of the initial hexagonal separatrix structure.

The toroidal field is assumed so strong that it is not perturbed by the plasma convection. Therefore, the toroidal field strength is simply

$$B_T(r,\varphi) = \frac{B_{TD}}{1+\frac{r}{R_D}\cos\varphi}\,, \tag{1}$$

where B_{TD} is the toroidal magnetic field at r=0. The poloidal flux function $\Phi(r,\varphi)$ for the standard, the snowflake, and the cloverleaf divertor is written as

$$\Phi^{(n)} = \frac{K_n}{n+1}\frac{B_{pm}}{a^n}r^{n+1}\sin(n+1)\varphi\,, \tag{2}$$

with n=1 for the standard null, n=2 for the snowflake, and n=3 for the cloverleaf. The parameter B_{pm} is the poloidal field strength at the separatrix at the midplane and a is the

minor radius. The dimensionless coefficient K_n is of order unity and depends on the global configuration. This parameter has been evaluated for specific configurations of standard and snowflake divertors in Ref. 16 and for a cloverleaf divertor in Ref. 17. The magnitude of K_n corresponding to the standard and the snowflake divertors are defined by Eqs. 10, 18, 19, and 23 and Table 1 of Ref. 16. They are: K_1=0.73 and K_2=0.57 for a "reference" geometry described in Ref. 16. For the cloverleaf divertor, we choose the configuration corresponding to the fourth line of Table 1 of Ref. 17 (it provides the largest distance from the PF coils to the null among all configurations considered in Ref. 17), yielding K_3=7.5. Note that the notation in Refs. 16-17 is different from that used in the present paper.

Although our general results cover all three of these divertors, in the specific examples we focus on the snowflake divertor.

3. The mode structure

A Lagrangian description is used where the initial position of the fluid element in the poloidal plane is characterized by the angle φ_0 with respect to the axis x, and the radius r_0. Each fluid element stays on the circle of the initial radius r_0 but moves along the circle by some angle, which depends on both r_0 and φ_0 , Fig. 2. In other words, the new position of the fluid element is related to the initial one by the following equations:

$$r = r_0 \tag{3}$$

$$\varphi = \varphi_0 + \chi(r_0) + \Delta\chi(r_0, \varphi_0) \ . \tag{4}$$

The term $\chi(r_0)$ corresponds to a uniform rotation at a given radius. As the azimuthal distance between two neighboring points would not change in such a displacement, it would cause a perturbation to the toroidal field, which is unacceptable. The last term in

Eq. (4) has to be adjusted in such a way that the toroidal magnetic field in the new location be equal to the pre-existing toroidal field in this location. From the flux conservation constraint, one finds:

$$B_T(\varphi)d\varphi = B_T(\varphi_0)d\varphi_0 \,. \tag{5}$$

Using Eqs. (1) and (5) and the smallness of r/R, one finds:

$$\Delta\chi(r_0,\varphi_0) = \frac{r_0}{R_D}\left[\sin\varphi_0 - \sin\left(\varphi_0 + \chi(r_0)\right)\right] \tag{6}$$

Note that this derivation does not assume a small displacement: the angle χ_0 is not assumed to be small compared to unity.

The mode has differential rotation where the fluid elements are displaced along circles, with the rotation angle varying along the radius and weakly varying along the azimuth ($\Delta\chi << \chi$). Equations (3), (4) and (6) serve as a basis for analysis of the change in a plasma thermal energy and magnetic energy caused by the churning mode

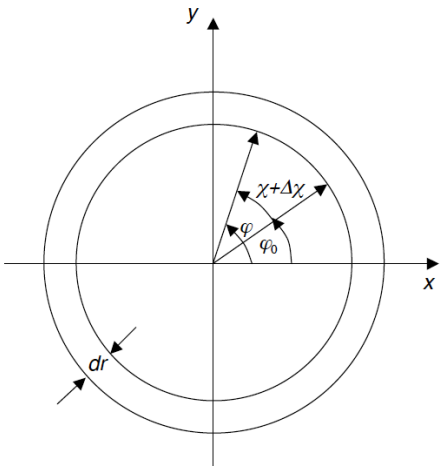

Fig. 2 Towards description of the churning mode. An annulus of a thickness *dr* is shown. Inside this annulus each point with the initial polar angle turns by some angle around the axis. The turn depends on the radius of the annulus, i.e., the twist is sheared.

4. Thermal energy release

The initial, unperturbed volume of a certain toroidal flux tube is $V_0 = 2\pi R_0 r_0 dr_0 d\varphi_0$, whereas its volume at the new location is $V = 2\pi R r_0 dr_0 d\varphi$. As the quantities d$\varphi$ and dφ_o are related by Eq. (5), one finds that

$$\frac{V}{V_0} = \frac{R^2}{R_0^2} = \frac{2r_0}{R_D}\left[\sin\varphi_0 - \sin\left(\varphi_0 + \chi(r_0)\right)\right], \tag{7}$$

where only zeroth- and first-order terms in the parameter r_0/R are retained. One can see that the relative change of the volume of the flux-tube contains a small parameter r_0/R, and accordingly, the change of the thermal energy for a toroidal annulus of a radius r_0 and a thickness Δr for a given $\chi(r_0)$ is:

$$\Delta W_T = \frac{4}{3}\frac{r_0^2 dr_0}{R_0}\int_0^{2\pi} p(r_0,\varphi_0)\left[\cos\varphi_0 - \cos(\varphi_0 + \chi(r_0))\right]d\varphi_0 \ . \tag{8}$$

This quantity is the energy of the annulus per unit length in the toroidal direction. We assume that the plasma behaves thermodynamically as an ideal monatomic gas.

The dependence of the churn angle χ on radius r will be used to evaluate the net energy available (thermal energy release minus the energy spent perturbing the poloidal magnetic field) to drive the convective motion in the PF null area.

Consider the particular case where the pressure is a linear function of the vertical coordinate y, with higher values of the pressure at larger y (closer to the confinement region) and lower values in the area where the plasma start flowing towards divertor targets along the divertor legs. In other words, assume that

$$p(r,\varphi_0) = const + p' r\sin\varphi_0 \ , \tag{9}$$

where the pressure gradient is assumed constant. The first term does not contribute to the energy release (8), whereas the second one does. One easily finds from Eq. (8) that

$$\Delta W_T = \frac{\pi r^3 \Delta r}{R} \frac{4p'}{3} \sin\chi(r_0) \ . \qquad (10)$$

In order to have thermal energy release ($\Delta W_T < 0$), the plasma should turn clockwise, χ<0 (using the standard convention that the geometrical axis is situated to the left of the poloidal cross-section as shown in Fig. 1). Note that by using Eq. (9) we have abandoned an assumption of p being a function of the flux surface that is usually used in the equilibria analyses based on Grad-Shafranov equations (see, e.g., Ref. 1). The assumption encapsulated in Eq. (10) may be more relevant to the problem of convective heat transport, with the value of p' being a control parameter that determines the intensity of the convective motion required to sustain a certain heat flux. We, however, are not attempting to solve a complete self-consistent problem and consider p' just as a given input parameter.

Qualitatively, the energy release is associated with the change of the volume of the toroidal flux tube as it moves to a larger major radius where the field is lower and the toroidal length is larger, leading to the release of thermal energy via adiabatic expansion. Note that the derivative $\left(\partial \Delta W_T / \partial \chi\right)_{\chi=0} = -\left(4\pi r^3 \Delta r / 3R\right) p'$ at χ=0 is non-zero for $p' \neq 0$, indicating the absence of equilibrium in this initial state.

5. Magnetic energy perturbation

Consider now the (stabilizing) magnetic energy perturbation. Here we neglect the small terms of order of r/R because the magnetic field perturbation occurs already in the zeroth order in this parameter. For 2D motion in the (r, φ) plane, the flux function is

advected by the fluid; for every parcel of the fluid, the value of the flux function remains equal to its initial value:

$$\Phi(r,\varphi) = \Phi_0(r_0,\varphi_0);\;\; r = r(r_0,\varphi_0); \varphi = \varphi(r_0,\varphi_0) \,. \tag{11}$$

For the churning mode in zeroth order in r/R, one has:

$$r = r_0;\;\; \varphi = \varphi_0 + \chi(r_0) \,. \tag{12}$$

Therefore,

$$\Phi = \Phi_0\left[r, \varphi - \chi(r)\right] \,. \tag{13}$$

The magnetic energy density is:

$$w_M = \frac{1}{8\pi}\left[\left(\frac{\partial\Phi}{\partial r}\right)^2 + \frac{1}{r^2}\left(\frac{\partial\Phi}{\partial\varphi}\right)^2\right] \,. \tag{14}$$

Accordingly, the change of the magnetic energy per unit toroidal length and annular width Δr is (for $r<<R$):

$$\Delta W_M = \frac{r\Delta r}{8\pi}\int_0^{2\pi}\left[\left(\frac{\partial\Phi_0(r,\varphi-\chi(r))}{\partial r} - \frac{d\chi}{dr}\frac{\partial\Phi_0(r,\varphi-\chi(r))}{\partial\varphi}\right)^2 + \frac{1}{r^2}\left(\frac{\partial\Phi_0(r,\varphi-\chi(r))}{\partial\varphi}\right)^2 - \left(\frac{\partial\Phi_0(r,\varphi)}{\partial r}\right)^2 - \frac{1}{r^2}\left(\frac{\partial\Phi_0(r,\varphi)}{\partial\varphi}\right)^2\right] d\varphi \tag{15}$$

To evaluate the magnetic energy for the three divertor configurations, we use Eq. (2). Because the integrand in Eq. (15) is periodic in φ, some cancellations occur, and the final result acquires the form

$$\Delta W_M = \frac{r\Delta r}{8\pi}\left(\frac{d\chi}{dr}\right)^2\int_0^{2\pi}\left[\frac{\partial\Phi_0(r,\varphi-\chi(r))}{\partial\varphi}\right]^2 d\varphi \,. \tag{16}$$

This expression can be applied to all three types of divertors, the standard null, the snowflake, and the cloverleaf. A simple integration for Φ_0 as in Eq. (2) yields:

$$\Delta W_M = \frac{\pi r^{2n+3} \Delta r}{a^{2n}} \left(\frac{d\chi}{dr} \right)^2 \frac{K_n^2 B_{pm}^2}{8\pi} . \qquad (17)$$

6. The size of the convection zone

To get a rough idea of the radius d of the zone encompassed by the churning mode and the temporal characteristics of the mode, we explore a specific type of differential rotation,

$$\chi = -\chi_0 \exp(-r^2 / d^2) \qquad (18)$$

The parameter d describes the size of the convection zone: the rotation must gradually vanish at larger radii due to a rapid growth of the magnetic energy perturbation. The parameter χ_0 characterizes the degree of rotation near the axis. In the initial state, before the motion starts, the rotation is zero. Substituting Eq. (18) into Eqs. (10) and (17), summing, and integrating over the radius, one finds the energy available for driving the churning mode:

$$W = -\int_0^\infty (\Delta W_M + \Delta W_T) dr = \\ -\frac{\pi K_N^2}{a^{2n}} \frac{B_{PM}^2}{8\pi} \int_0^\infty r^{2n+3} \left(\frac{\partial \chi}{\partial r} \right)^2 dr - \frac{\pi}{R} \frac{4p'}{3} \int_0^\infty r^3 \sin\chi \, dr \qquad (19)$$

A positive sign for W indicates that the thermal energy release overweighs the magnetic energy increase, and the mode can be excited. This requires $\chi_0 < 0$, i.e., a clockwise rotation.

In the first integral in Eq. (19), integration is elementary, yielding

$$\int_0^\infty r^{2n+3} \left(\frac{\partial \chi}{\partial r} \right)^2 dr = \frac{\chi_0^2 d^{2n+2} (n+2)!}{2^{n+2}} . \qquad (20)$$

The second integral can be written as

$$\int_0^\infty r^3 \sin\chi dr = d^4 F(\chi_0) \,. \tag{21}$$

where the function $F(\chi_0)$ is

$$F(\chi_0) = \int_0^\infty x^3 \sin\left(\chi_0 e^{-x^2}\right) dx \,. \tag{22}$$

The plot of this function is shown in Fig. 3.

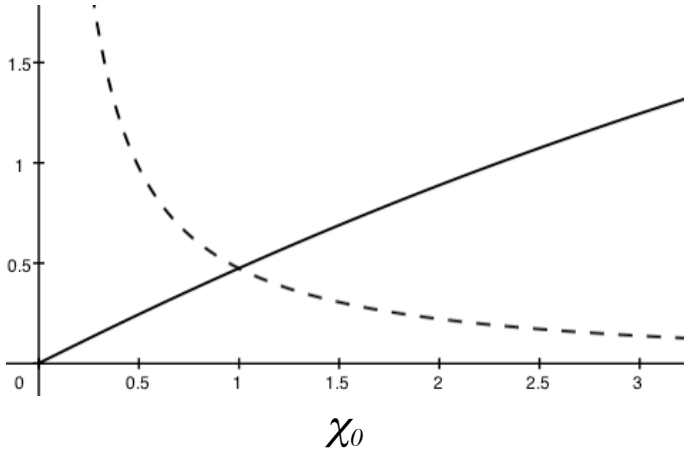

Fig. 3 The functions $F(\chi_0)$ (solid line) and $F(\chi_0)/\chi_0^2$ (dashed line) that enter Eqs. (21) and (24); χ_0 is measured in radians.

As the derivative of the thermal drive at χ_0=0 is non-zero, the initially resting plasma starts clockwise rotation. The kinetic energy for the mode (18) is:

$$W_{kin} = \pi\rho \int_0^\infty r^3 \dot{\chi}^2 dr = \pi\rho\dot{\chi}_0^2 \int_0^\infty r^3 e^{-2r^2/d^2} dr = \frac{\pi}{8}\rho\dot{\chi}_0^2 d^4 \tag{23}$$

(per unit length in the toroidal direction). We assume here a uniform density distribution. The rotation amplitude $|\chi_0|$ initially grows, but then the magnetic energy becomes comparable to the thermal energy, and rotation stops at some $|\chi_0| = \chi^*$. After reaching this point, the rotation reverses sign, the plasma returns to the initial state of χ_0=0, etc. A

shape of the potential well in which these oscillations occur is illustrated by Fig. 4a for the case where $|\chi^*|=\pi$. The dynamics of this process can be found from equation $W_{kin}=W$ (see Section 7). The maximum rotation angle is determined from the condition $W(\chi^*)=0$. A large-enough maximum rotation angle provides a mechanism for heat exchange by mixing the hotter and colder plasmas.

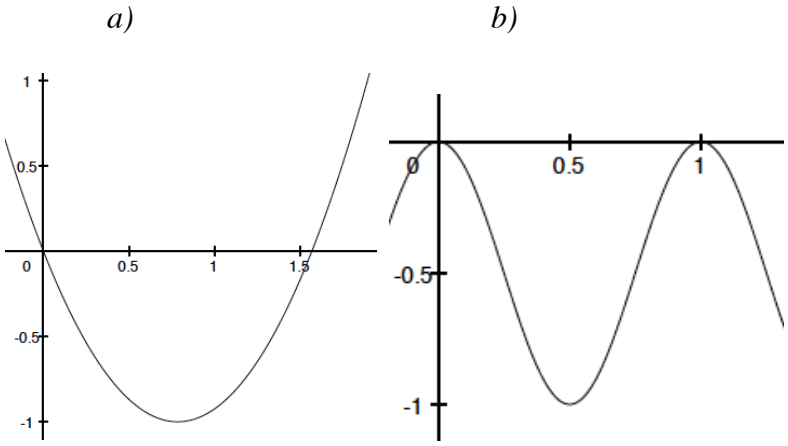

Fig. 4 Dynamics of the system: a) Potential energy dependence on $-\chi_0$ (in radians). The energy is normalized to make its minimum equal to -1. The system starts at a zero velocity at χ_0 =0 and oscillates between two turning points; b) Rotation angle in the units of π vs. time (normalized to the period τ).

One can visualize the evolution of the poloidal magnetic field by following the flux surfaces that formed a hexagonal separatrix in the initial state; this is illustrated by Fig. 5. The perturbation of the poloidal magnetic field is of order of the initial field. For panels c and d in Fig. 5, the plasma mix is quite substantial.

Let's find the conditions under which the maximum turn angle is $|\chi^*|=\pi$, i.e., by requiring that W in Eq. (19) is zero for $\chi_0 = \pi$. This condition means that the mode can turn the plasma in the convection zone "upside down", bringing the hottest part (initially

at the top) to the bottom, which is in contact with the plasma exhaust channels and activating additional channels in the cases of a cloverleaf and a snowflake.

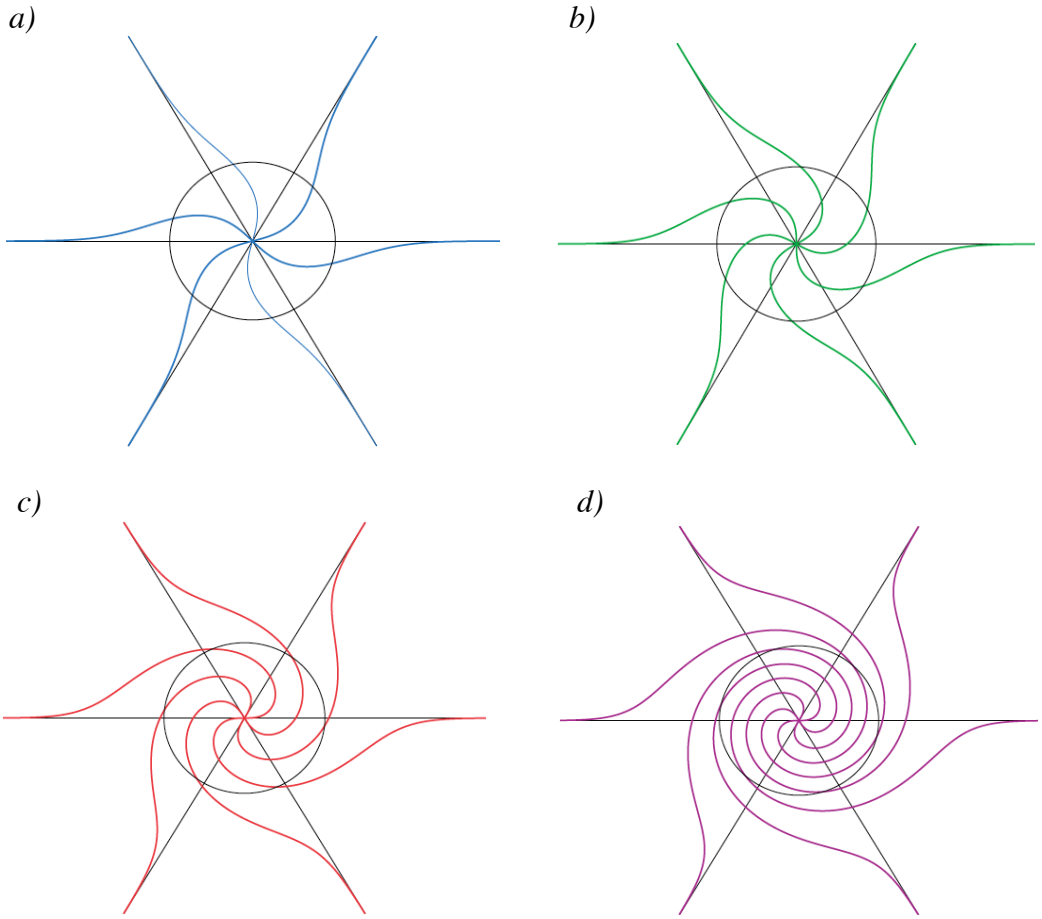

Fig. 5 Evolution of the separatrix entrained by the churning mode. The coordinates are normalized to d, with the circle having a radius of the unity. Black straight lines indicate six branches of the unperturbed snowflake separatrix. The upper left panel corresponds to initial state, upper right panel, to $\chi_0=\pi/2$, the lower left panel corresponds to our reference case of the upside-down turn, and the lower right panel corresponds to a stronger drive, where a full 2π turn becomes possible. The cross-field transport is greatly facilitated for the lower panels.

For $\chi*=\pi$, the required condition acquires the form:

$$\frac{d}{a}=\left(\beta_p\frac{a}{R}\right)^{\frac{1}{2n-1}}\left(\frac{2^{n+4}F(\chi^*)}{3K_n^2\chi^{*2}(n+2)!}\right)^{\frac{1}{2n-1}},\quad \chi^*=\pi\ . \tag{24}$$

We have introduced a parameter

$$\beta_p = \frac{8\pi \mid p' \mid d}{B_{pm}^2} \tag{25}$$

that characterizes the plasma pressure in the convection zone relative to the poloidal field pressure at the midplane SOL. As the pressure drop across the SOL is of order of the pressure, we assume $\mid p' \mid d \sim p$ for numerical estimates. Using the numerical values of the coefficients, we find

$$\frac{d}{a} = 0.44 \beta_p \frac{a}{R} \tag{26}$$

for a standard divertor,

$$\frac{d}{a} = 0.71 \left(\beta_p \frac{a}{R} \right)^{\frac{1}{3}} \tag{27}$$

for a snowflake divertor, and

$$\frac{d}{a} = 0.24 \left(\beta_p \frac{a}{R} \right)^{\frac{1}{5}} \tag{28}$$

for a cloverleaf divertor. As the parameter $\beta_p(a/R)$ is usually small (see Table 1), the convection zone size is significantly larger for the snowflake and the cloverleaf divertors than for the standard one. Typically, for the standard divertor, the ratio of d/a evaluated from Eq. (26) is on the order of 1/200 – 1/300. Any significant changes of the equilibrium in the divertor area of the standard divertor and even more so the hypothesized onset of the churning motion would require unrealistically high plasma pressures near the edge. Not surprisingly, no twisting of the field lines of the type illustrated in Fig. 5 shows up in the available analyses of the plasma equilibria (see Ref. 18 and references therein).

Conversely, for the snowflake divertor the ratio d/a is of the order of (1/10-1/5)a and should have a much stronger impact. For the cloverleaf, the "churning" zone is

approximately the same, due to the small numerical coefficient in Eq. (28). In the next sections we will focus therefore on the snowflake (n=2).

An important issue is that of the size of the convective zone as projected along the poloidal field flux surfaces to the midplane. Outside the convective zone these surfaces stay unperturbed and are therefore well defined. In the snowflake geometry, the flux surface whose shortest distance to the null is d, the magnetic flux is (see Eq. (2) and Ref. [16]) $\Phi_d = 0.19a(d/a)^3 B_{pm}$ per unit length in the toroidal direction. For $\chi^*=\pi$ this corresponds to the midplane width

$$\frac{\Delta}{a} = 0.19\left(\frac{d}{a}\right)^3 \approx 0.07\beta_{pm}\frac{a}{R} \tag{29}$$

of the zone affected by the convection both inside and outside the separatrix. [We neglect here the difference of the major radii between the poloidal field null and the midplane SOL.]

7. Mode dynamics

To find the period of this mode, one can use the energy conservation equation, $W=W_{kin}$, that allows one to relate $\dot{\chi}_0$ and χ_0, as in the standard theory of a non-linear oscillator. Then, the temporal dependence of χ_0 can be found by an integration of $dt = d\chi_0/\dot{\chi}_0$ over χ_0. The plot of χ_0 vs. time is shown in Fig. 4b. The period of oscillations for the snowflake divertor is

$$\tau = \frac{1.3\sqrt{Rd}}{\sqrt{2T/m_i}} \tag{30}$$

For larger plasma pressures, larger amplitude of oscillations becomes possible, reaching 2π and even higher values. Heat transport holds the gradient down, providing a self-regulating mechanism (which we do not analyze in this paper).

It is instructive to compare the churn time (30) with the diffusion time corresponding to the Bohm diffusion coefficient:

$$\tau_B \sim \frac{d^2}{2D_B} \quad . \tag{31}$$

where $D_B = (1/16)(cT/eB_T)$ (or, numerically, $D_B(cm^2/s) \approx 600T(eV)/B(T)$. Taking, as an example, T=50 eV, B=2 T, d=10 cm, one finds $\tau_B \sim 6 \cdot 10^{-3}$ s, whereas the "churn" time (30) is $\sim 10^{-5}$ s, i.e., much shorter.

Another important parameter that is related to the effect of the mode on divertor performance, is the transit time of the plasma in its flow along field lines to the divertor targets. In order for convection to be effective in spreading the heat, the period τ, Eq. (30) should be shorter than the transit time $\tau_{\|d}$ through the divertor region. For the latter we take the transit time for the field lines that just skirt the convective zone passing at a minimum distance d from the null. As the end-points we take the points that corresponds to the field strength that is 2 times higher than the field at the point of the closest approach (Fig. 6). Simple calculations show that this connection length is (see Ref. 16)

$$\ell_{\|d} = 0.7 \frac{a^2}{d} \frac{B_T}{B_{pm}} . \tag{32}$$

For the reference parameters of Table 1, this is 10^{-4} s, i.e., much longer than the time τ. This disparity would become even stronger for the field line that passed closer to the null in the unperturbed state. In other words, the plasma flow is indeed strongly mixed near

the null before passing further to the divertor legs. Parallel heat conduction may also contribute to the heat flux. For our reference parameters the effect of the convective zone on this component of the flux is equally strong.

To evaluate the applicability of the frozen-in condition that we have been using in the analysis of the magnetic field perturbations, we calculate the magnetic Reynolds number, the ratio of the magnetic diffusion time to the oscillation period τ:

$$\mathrm{Re}_M = \frac{d^2}{2D_M \tau} \tag{33}$$

The magnetic diffusivity can be evaluated as $D_M(cm^2/s) \sim 4 \cdot 10^6 / \left[T_e(eV)\right]^{3/2}$. Taking the plasma temperature to be 50 eV and d=10 cm, we find that Re_M~600. This means that the line-tying holds with high accuracy.

The field structures shown in Fig. 5c are usually prone to reconnection, but the field strength of the poloidal field is small, with magnetic pressure being much smaller than the plasma pressure in the convection zone. The assessment of reconnection in this peculiar situation would require a separate analysis.

One cannot rule out that after a few bounces the churning mode will settle down at the equilibrium that looks like the structure shown in Fig. 5c or similar. This scenario, however, seems to be rather improbable due to the complexity of the field structure prone to reconnections and smaller-scale instabilities in a medium with a steep variation of the plasma parameters. On the other hand, in the transition zones with distance from the null somewhat higher than d, slightly twisted equilibria similar to those shown in Fig. 5a may be possible.

8. Discussion

In the previous sections a semi-quantitative analysis of the plasma dynamics in the zone near the poloidal field null has been presented. The characteristic size of the zone where this mode can emerge has been estimated. It turned out that for the standard divertor it is very small, a fraction of a centimeter for parameters typical of existing fusion facilities. Conversely, for the snowflake and cloverleaf configurations the size of the zone can be significant. The further discussion will focus on the snowflake divertor because it has already been realized on several tokamaks [10-14].

The predicted size of the convection zone for these facilities is typically on the order of 1/10 of the plasma minor radius for the inter-ELM plasmas. The convection diverts part of the heat flux into the two divertor legs that initially are not in contact with the SOL plasma. This feature has been particularly clearly demonstrated in the TCV experiments [11, 14].

Table 2. Derived parameters for the "generic" tokamak of Table 1

Parameter	Plasma beta	Size of convection zone	Turn-over time	Bohm time	Parallel transit time	Magnetic diffusion time
Notation and Eq. number	β_{pm}, Eq. (25)	d, Eq. (27)	τ Eq. (30)	τ_B Eq. (31)	$\tau_{\parallel d}$ Eq.(32)	τ_m Eq.(33)
Value	$6\cdot10^{-3}$	10 cm	7 μs	3 ms	0.3 ms	4ms

The churning mode, by its very nature, involves not only a SOL and initial private flux region, but also the bottom of the confinement zone (see Fig. 1). However, the poloidal magnetic flux threading this zone is approximately the same as the flux

threading the SOL and, when projected to the midplane, corresponds to the distance from the separatrix of only a few millimeters. In terms of the core plasma confinement, this is like shifting the separatrix inward by this distance and, thereby, losing a few percent of the plasma volume. The effect can be described as the effect of inserting a smooth, distributed limiter inside the separatrix. Experimentally, there have been no observations indicating any deterioration of the core plasma confinement in the presence of the heat flux splitting between several divertor legs [10-14].

In our discussion, we considered an exact snowflake configuration, whereas in real experiments one usually deals with an "approximate" snowflake, where instead of one second-order null one deals with two closely spaced first-order nulls. Our description will still be applicable to this latter situation if the distance between the nulls is smaller than the size of the convection zone evaluated from Eq.(27). This is one of the "proximity constraints" that make an approximate snowflake act similarly to the exact one [4].

The convection should become particularly strong during the ELM events when the plasma pressure in the SOL increases by a factor of 10 to 30 compared to the inter-ELM periods [19]. The higher pressure increases the size of the zone and provides conditions for a strong heat flux between the divertor legs. This was observed on TCV, NSTX and DIII-D [10-14]. A detailed experimental study has been performed on TCV [14].

Other mechanisms that may lead to enhanced heat transport in the null area are hydrodynamic instabilities with the cross-field scale much smaller than d studied in Ref. 6, 7 and the electric drifts caused by the ambipolar electric field.

Among the MHD instabilities [6, 7] the most efficient one is a toroidally-symmetric quasi-flute mode [6] that develops on the background of the initial equilibrium. It favors those parts of the initial equilibrium configuration where the unperturbed pressure gradient is directed towards the geometrical axis. The instability conditions analyzed in Ref. 6 can be satisfied in some areas of all three experimental facilities (TCV, NSTX and DIII-D). The ballooning mode may also play some role, especially during the ELM events [7].

The effect of electric drift has been first analyzed for the standard divertor [8]. It may produce a convection pattern similar to that of the churning mode, although it is purely electrostatic and does not perturb the magnetic field. For the snowflake geometry a similar mechanism was assessed in [9]. The convection velocity produced by the ambipolar field is typically smaller than that produced by the churning mode. On the other hand, it can act at low plasma pressures, when the churning mode is inefficient.

In reality, one will probably have an interplay of all the mechanisms mentioned above. To reach a better understanding of the MHD effects, numerical simulations of the type that can be performed by the NIMROD code [20] would be desirable. With regard to the churning mode, effects of magnetic reconnection on the well-developed convection would be important to assess.

In summary: A semi-quantitative analysis of a churning mode in the area of a weak poloidal magnetic field near the second-order null has been presented. The mode generates a poloidal rotation of plasma that flips the plasma distribution upside-down and brings the warmer plasma directly to the private flux area, thereby activating additional divertor legs.

Acknowledgment

This work was performed under the auspices of the U.S. Department of Energy by Lawrence Livermore National Security, LLC, Lawrence Livermore National Laboratory, under Contract DE-AC52-07NA27344.

References

1. V. D. Shafranov, Reviews of Plasma Physics, edited by M. A. Leontovich (Consultants Bureau, New York, 1966), Vol. 2, p. 103.

2. D.D. Ryutov and T.D. Rognlien, "Using the snowflake geometry to mitigate pulsed divertor heat loads during the ELM events" Paper 3O3 at the Int. Sherwood Fusion Theory Conference, Austin, TX, May 2-4, 2011.

3. D. D. Ryutov, R.H. Cohen , T.D. Rognlien and M. V. Umansky. "Plasma convection near the magnetic null of a snowflake divertor during an ELM event." Contrib. Plasma Phys., **52**, No. 5-6, 539 – 543, 2012.

4. D. D. Ryutov, R.H. Cohen, T.D. Rognlien and M. V. Umansky. "A snowflake divertor: solving a power exhaust problem for tokamaks." PPCF, **54**, 124050, 2012.

5. D.D. Ryutov, R.H. Cohen, E. Kolemen, L. LoDestro, M. Makowski, J. Menard, T.D. Rognlien, V.A. Soukhanovskii, M.V. Umansky, X. Xu. Theory and Simulations of ELM Control with a Snowflake Divertor. TH/P4-18

6. W.A. Farmer, D.D. Ryutov. "Axisymmetric curvature-driven instability in a model divertor geometry." Phys. Plasmas, **20**, 092117, September 2013.

7. W.A. Farmer. "Ballooning modes localized near the null point of a divertor." Subnitted to Phys. Plasmas, January 2014.

8. M.J. Schaffer, J.A. Boedo, R.A. Moyer, T.N. Carlstrom, J.G. Watkins. "Large EXB convection near the divertor X-point." JNM, **290-293**, 530 (2001).

9. G.P.Canal et al."Comparison between experimentsand EMC-3-Eirene simulationsof the snowflake divertor in TCV. BAPS, **58**, #16, p. 256.

10. V. A. Soukhanovskii, J.-W. Ahn, R. E. Bell, D. A. Gates, S. Gerhardt, R. Kaita, E. Kolemen, B. P. LeBlanc, R.Maingi, M. Makowski, R. Maqueda, A.G. McLean, J. E. Menard, D. Mueller, S. F. Paul, R. Raman, A. L. Roquemore, D. D. Ryutov, S.A. Sabbagh, H. A. Scott. "Taming the plasma-material interface with the 'snowflake' divertor in NSTX," Nucl. Fus., **51**, 012001 (January 2011).

11. W.A.J. Vijvers, G.P. Canal, B. Labit, H. Reimerdes, B. Tal, S. Coda, B.P. Duval, T. Morgan, G. de Temmerman, J.J. Zielinski and the TCV team. "Reduction of Peak Wall Power Loads in L- and H-mode Tokamak Plasmas in TCV with the Snowake Divertor." Paper EX/P5-22 at 2012 IAEA Fusion Energy Conference, San-Diego, October 8-12, 2012
http://www-naweb.iaea.org/napc/physics/FEC/FEC2012/papers/490_EXP522.pdf

12. S. L. Allen, V. A. Soukhanovskii, T.H. Osborne, E. Kolemen, J. Boedo, N. Brooks, M. Fenstermacher, R. Groebner, D. N. Hill, A. Hyatt, C. Lasnier, A. Leonard, M. Makowski, W.H. Meyer, A. McLean, T. Petrie, D. Ryutov, J. Watkins. "Results From Initial Snowflake Divertor Physics Studies on DIII-D," Paper PD/1-2, IAEA Fusion Energy Conference, San Diego, CA October 8-12, 2012.

13. H Reimerdes, G P Canal, B P Duval, B Labit, T Lunt, W A J Vijvers, S Coda, G De Temmerman, T W Morgan, F Nespoli, B Taland the TCV Team. "Power distribution in the snowflake divertor in TCV." Plasma Phys. Control. Fusion **55** (2013) 124027

14. W A J Vijvers, Gustavo P Canal, Benoit Labit, Holger Reimerdes, Balasz Tal, Stefano Coda, Gregory De Temmerman, Basil P Duval, T W Morgan, Jakub Jedrzej Zielinski and the TCV team. "Power exhaust in the snowflake divertor for L- and H-mode TCV tokamak plasmas." Nuclear Fusion, **54**, February 2014.

15. Tilmann Lunt, Gustavo P Canal, Yuhe Feng, Holger Reimerdes, Basil P Duval, Benoit Labit, W A J Vijvers, David P Coster, Karl Lackner and Marco Wischmeier. "First Edge Monte Carlo 3D-Eirene simulations of the TCV snowflake divertor." PPCF, **56**, March 2014.

16. D.D. Ryutov, R.H. Cohen, T.D. Rognlien, M.V. Umansky. "Magnetic field structure of a snowflake divertor." Phys. Plasmas, **15**, 092501 (2008).

17. D.D. Ryutov, M.V. Umansky. "Divertor with a third-order null of the poloidal field." Phys. Plasmas, **20**, 092509 (2013).

18. A. J. Cerfon and J. P. Freidberg "'One size fits all' analytic solutions to the Grad–Shafranov equation", Phys. Plasmas, **17**, 032502, 2010.

19. D.N. Hill. "A review of ELMs in divertor tokamaks. "Journ. Nucl. Materials, **241**, 182, 1997.

20. C.R. Sovinec, A. H. Glasser, T. A. Gianakon, D. C. Barnes, R. A. Nebel, S. E. Kruger, D. D. Schnack, S. J. Plimpton, A. Tarditi, M. S. Chu, and the NIMROD Team, "Nonlinear magnetohydrodynamics simulation using high-order finite elements," J. Comput. Phys., **195**, 355 (2004)